Dyes and Pigments 182 (2020) 108625

Contents lists available at ScienceDirect

Dyes and Pigments

journal homepage: http://www.elsevier.com/locate/dyepig

Thermo-optic response of MEH-PPV films incorporated to monolithic Fabry-Perot microresonators

J. Gil Rostra [a,**], K. Soler-Carracedo [b], L.L. Martín [b], F. Lahoz [b], F. Yubero [a,*]

[a] Instituto de Ciencia de Materiales de Sevilla (CSIC – Univ. Sevilla), C/ Américo Vespucio 49, E-41092, Sevilla, Spain
[b] Departamento de Física, IUdEA, Universidad de La Laguna, Santa Cruz de Tenerife, Spain

ARTICLE INFO

Keywords:
Thermo-optic coefficient
Optical temperature sensor
MEH-PPV
Fabry-perot microresonator

ABSTRACT

Poly[2-methoxy-5-(2′-ethylhexyloxy)-1,4-phenylene vinylene] (MEH-PPV) is a semiconducting optically active polymer widely used in optoelectronics research. MEH-PPV can be commercially acquired in a large range of molecular weights. However, the influence of this property on the optical performance of the polymer is often disregarded. In this paper, the thermal dependence of the refractive index of MEH-PPV thin films prepared from high and medium molecular weight polymers is investigated. Thus, monolithic Fabry-Perot (FP) microcavities are fabricated, in which the active polymer film is part of their defect layer. It is found that when these devices are used as optical temperature sensors, the position of the emission band of the microcavities excited with a blue diode laser shifts to lower wavelengths when temperature increases with sensitivities in the 0.2–0.3 nm/°C range. This effect is ascribed to the variation in the refractive index of the polymer active layer within the resonator with temperature. According to theoretical simulations of optical transmittance by classical transfer-matrix method and the evaluation of the optical eigenmodes by finite element methods of the manufactured FP resonator cavities, it is found that the MEH-PPV films present negative thermo-optic coefficients of about $-0.018\ K^{-1}$ and $-0.0022\ K^{-1}$ for high and medium molecular weight polymers, respectively, in the temperature range between 20 and 60 °C. These values are about the highest reported so far, to the best of our knowledge, and points to high performance thermal sensor applications.

1. Introduction

Conjugated polymers have attracted great scientific and industrial attention since the pioneering report of organic light emitting diodes [1]. Their outstanding optoelectronic properties make them appealing materials for a wide range of applications, such as displays, waveguides, lasers, and photovoltaics [2–6]. Big efforts have been devoted to improve synthetic organic chemistry procedures that enable the versatility of this kind of materials for those applications [7,8]. In particular, the optical properties of conjugated polymers are of the highest importance for their final applications [9,10]. In this regard, some reports on basic optical properties of conjugated polymers show significant discrepancies [10,11]. It has been demonstrated that these disagreements may be related to the average molecular weight of the polymers used in the studies. Indeed, this property has a strong influence on the morphology and optoelectronic properties of conjugated polymer thin films [11,12].

In particular, the temperature dependence of the refractive index of the components of optically active thermal sensors, described through their thermo-optic coefficient, is of foremost importance. However, very often there is lack of information about this property [13,14]. In this context, poly(1-methoxy-4-(2-ethylhexyloxy)-*p*-phenylenevinylene) (MEH-PPV) is one of the light emitting conjugated polymers most often used in academia, research activities and proof-of-concept devices, being considered as a model material to illustrate the underlying physics of these materials [15,16]. It has been reported that, when MEH-PPV is prepared as thin film, its molecular weight has a deep influence on the refractive index and birefringence of the films.

In this paper, we report on the fabrication and thermo-optical response of compact monolithic 1D Fabry-Perot (FP) microresonators, in which MEH-PPV thin films are incorporated within the corresponding resonant cavities. Our results show that MEH-PPV thin films prepared with high molecular weight polymers have higher thermo-optic coefficient than those prepared with medium molecular weight ones,

* Corresponding author.
** Corresponding author.
E-mail addresses: jorge.gil@icmse.csic.es (J. Gil Rostra), yubero@icmse.csic.es (F. Yubero).

https://doi.org/10.1016/j.dyepig.2020.108625
Received 23 April 2020; Received in revised form 8 June 2020; Accepted 8 June 2020
Available online 28 June 2020

showing, to the best of our knowledge, the highest thermo-optic coefficient reported so far.

2. Experimental

2.1. Microresonator device fabrication

Several multilayer FP microresonator cavities were built on top of *BK7* glass substrates following the scheme drawn in Fig. 1a. They consisted of a spin coated MEH-PPV active polymer layer sandwiched between two Bragg mirrors (BM). The BMs were designed to behave as short-pass filters with a sharp transition edge between the absorption and emission bands of the active polymer at ~550 nm, to allow the optical excitation of the dye for wavelength below 550 nm and, at the same time, to enhance and filter its emission within the designed Fabry-Perot microcavity above 550 nm. The lower/upper reflector *BM1/BM2* was designed with 95/99% reflectance at the 630–670 nm wavelength range to enhance emission through the front side of the resonator. The first *BM1* was built by a sequence of seven periods of a *LHL* layered structure (*L* and *H* represent low and high refractive index materials, respectively) on top of a *BK7* coverslip. As *L* layers we used 39 nm thick SiO_2 (refractive index 1.45), and as *H* layers 88 nm thick Nb_2O_5 (refractive index 2.30), both prepared by reactive magnetron sputtering. Then a defect layer, *D*, which acts as the cavity of the resonator and comprises the polymer thin film was deposit. This *D* layer consisted of 1–3 spin coated MEH-PPV layers sandwiched between accommodation *L1* layers made of SiO_2. The total thickness of the *D* layer was about 600 nm. On top of this *D* layer, the second *BM2* consisted in a sequence of 5 periods of *LHL* structure. Thus, the complete multilayer of the microresonator was *BK7*(substrate)/$(LHL)^7/D/(LHL)^5$.

Monolithic microresonators were fabricated using two series of configurations for the cavity always with a total thickness around 600 nm, where MEH-PPV polymer layers were sandwiched between SiO_2 layers. In the first one, named as *conf-1H*, the active layer consisted of a spin coated thin film of high molecular weight MEH-PPV ($M_w > 100$ kg/mol, toluene solvent, @500 rpm during 1 min). Fig. 1b shows a cross section SEM image of one of these *D* cavities, where the polymer layer is placed as a central layer of about 25 nm (±2 nm errorbar) within the cavity. It is worth mentioning that the transmittance spectra of a single layer of MEH-PPV deposited on glass (see Fig. S1 in the Supporting Information file) was consistent with this thickness, considering the absorption coefficient of 18×10^4 cm^{-1} reported in the literature [12]. Other *conf-1H* samples were also produced with the polymer layer at different positions within the *D* cavity. In the second series of configurations, *conf-2M*, the active layer consisted of spin coated thin films of medium molecular weight MEH-PPV polymer (M_w = 40–70 kg/mol, toluene solvent, 30 mg/ml, @ 3000 rpm during 1 min). Fig. 1c shows a cross section SEM image of one of these *D* cavities, consisting in three polymer layers, with ~110 nm thickness each, and two accommodation SiO_2 layers, in between, representative of these manufactured *conf-2M* resonators. Fig. 1d shows a SEM cross section of the same complete *conf-2M* multilayer resonator. Other *conf-2M* resonators were also manufactured with different distribution of the polymer layer within the *D* cavity. The reason for the series of manufactured *conf-1H* and *conf-2M* samples with different polymer film distribution within the resonator cavity was to test the influence of electric field standing waves within the cavity in the thermo-optical response of the active MEH-PPV polymer.

2.2. Optical characterization

The reflectance at normal incidence of the individual manufactured *BM1* and *BM2* Bragg mirrors is shown in Fig. 2a. On the other hand, the absorbance (dashed line) and emittance (full line) of a single MEH-PPV film, expressed in arbitrary units, are shown in Fig. 2b. Note the high transmittance of the individual mirrors at wavelengths corresponding to the absorption band of the polymer.

The emission spectra were obtained by exciting with a continuous-wave blue diode pumped solid state laser at 473 nm with an incidence angle of 30° with respect to the normal of the multilayer resonator. The pump beam was collimated (around 1 mm diameter). Two linear crossed polarizers were used to reduce the pump density to about 1 mW/mm^2 to avoid laser induced heating. The sample was placed in thermal contact with a heatable plate. The temperature was varied between 20 and 60 °C to avoid the reported glass transition temperature for this polymer at 65 °C [17]. It was controlled with a type K thermocouple. A transparent cover was used to minimize heating losses. The emission was detected at the normal direction of the sample using an optical fiber coupled to the spectrometer (Andor SR-500i-B2) and the CCD detector (Newton 970EMCCD). Fig. 2c shows an example of the emission spectra (full red line) acquired in these conditions compared to the transmittance (dashed line) of the complete *conf-1H* resonator. The dotted vertical line in this figure indicates the excitation wavelength. On the other hand, a scheme of the experimental set-up is depicted in Fig. 3. The uncertainty of the detection system for the determination of the position of the emission band was 0.01 nm, experimentally evaluated as the standard

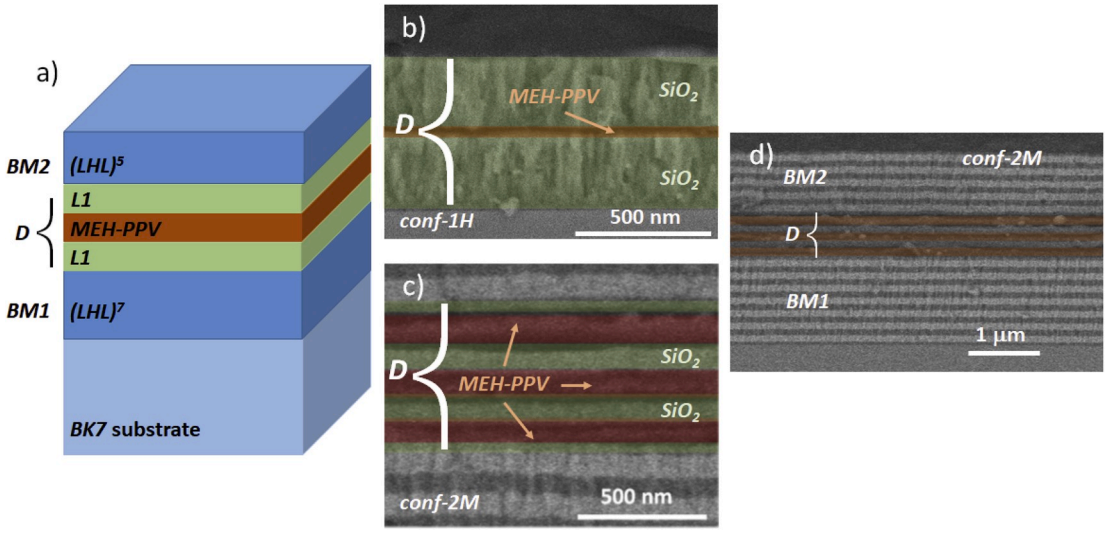

Fig. 1. (a) Multilayer scheme of the monolithic microresonators. (b) and (c) Cross section SEM images of the *D* cavity of *conf-1H* and *conf-2M* monolithic resonators, respectively. (d) Full *conf-2M* resonator.

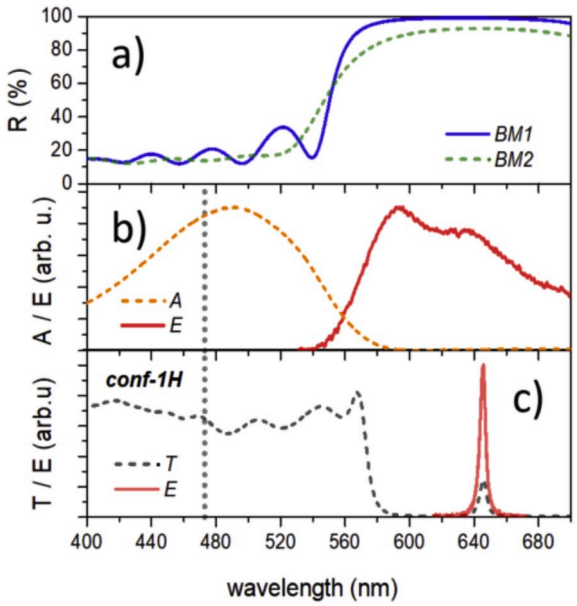

Fig. 2. (a) Reflectance of the individual *BM1* and *BM2* Bragg mirrors. (b) Absorbance (dashed line) and emission (full line) expressed in arbitrary units of a single MEH-PPV film. (c) Transmittance (dashed line) and emission (full line) spectra of the complete *conf-1H* resonator. The dotted vertical line indicates the excitation wavelength.

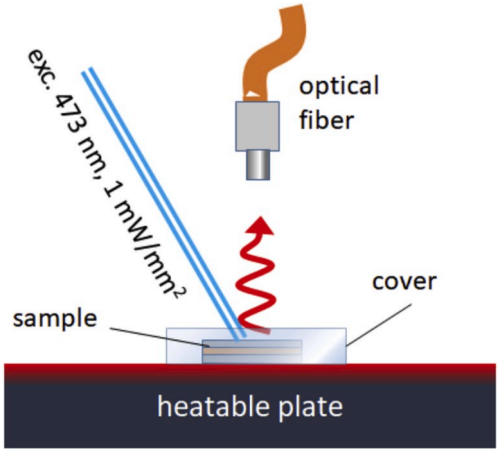

Fig. 3. Scheme of the setup used for the temperature dependent emission experiments.

deviation of the spectral position distribution obtained from the fitting of 100 spectra acquired under the same laboratory conditions.

3. Results

3.1. Characterization of the temperature optical sensor

In this section, we focus on the emission properties of the MEH-PPV semiconducting polymers incorporated to the microresonators and their temperature dependence.

The emission of the microresonators was detected at the normal direction of the device under excitation at 473 nm, close to the maximum of the polymer absorption band. The recorded spectrum consists of narrow bands (FWHM 4.2 nm and 7.0 for *conf-1H* and *conf-2M*, respectively) as compared to the broader emission band of the native film (FWHM about 80 nm, see Fig. 2b). Both the narrowing of the emission band of the polymer and its spectral position are determined by the optical characteristics of the monolithic Fabry-Perot resonator. The multilayer structure of the device tune the position of the allowed transmission band within the optical gap of the BMs and, at the same time, the allowed optical states within the manufactured 1D photonic crystal. Indeed, the position of the emission bands of the MEH-PPV microresonators evaluated at room temperature coincide with those of its transmission spectrum (cf. Fig. 2c). However, their widths were slightly narrower than those of the corresponding transmission spectra (FWHM 4.9 nm and 7.6 nm for *conf-1H* and *conf-2M*, respectively). Thus, the Q-factor of *conf-1H* resonators take values around 150, while those of *conf-2M* resonators take values around 90.

The experimental emission spectra acquired for temperatures between 20 and 60 °C are shown in Fig. 4a and b for the *conf-1H* and *conf-2M* microcavities, respectively. A reversible blue shift of the resonant peaks $\Delta\lambda_p$ of up to ~10 nm (*conf-1H*) and ~7 nm (*conf-2M*), was observed for a temperature increment of 32 °C, as it is reported in Fig. 4c. The resonance blue shifts were not linear with temperature showing higher slope at lowest temperatures. The average resonance shift of −0.22 and −0.31 nm/°C for the medium and high molecular weight samples, respectively, can be considered as a measurement of the temperature sensitivity of the microresonators acting as optical temperature sensors. The absolute values of this sensitivities are remarkably higher than those reported for other optical sensors. For example, an average resonance shift of 0.032 nm/°C has been reported in a glass based FP optofluidic microresonator [18], 0.01 nm/°C shift was found in whispering gallery modes (WGM) on a glass fiber [19], 0.15 nm/°C emission shift was detected in a near-infrared FP optofluidic microresonator [20], 0.11 nm/°C was reported in a small 4 μm diameter silicon ring resonator [21], and the highest value of 0.245 nm/°C was found in high-Q WGM Poly(dimethylsiloxane) microsphere resonators [22]. The shifts of the resonant wavelengths with temperatures found in the developed *conf-1H* and *conf-2M* resonators, comprising high and medium molecular weight MEH-PPV active polymers respectively, are among the highest shifts ever reported.

The limit of detection (LOD) of the sensor, ΔT_{min}, also known as temperature resolution, is the smallest change in temperature that can be detected. It is given by the ratio of the uncertainty of the detection system for the determination of the position of the emission band (0.01 nm in our experiments, c.f. experimental section) to the rate of change of the position of the resonant peak with temperature, $d\lambda_p/dT$. It can be numerically calculated from the data shown in Fig. 4c.

Fig. 4d shows the LOD of the microcavities acting as optical temperature sensors with high and medium average molecular weight MEH-PPV polymer layers incorporated to *conf-1H* and *conf-2M* structures. The combination of relatively high sensitivities together with the small uncertainty in the determination of the peak resonance provides the LOD values reported in Fig. 4d. These values are smaller than those found using other techniques, such as fluorescence intensity ratio [23–25]. Conventional optical fiber temperature sensors are grounded on light interference and typical temperature resolution below 1 °C was reported [26]. A very small value of temperature resolution, about 10^{-4} °C, was reported for high-Q PDMS WGM resonators [22]. However, in that case a tunable, narrow linewidth external-cavity laser is used to analyze the PDMS microspheres and the laser light had to be coupled into the microsphere through a fiber taper. On the other hand, in our experimental setup the microcavity can be interrogated with a cheap diode laser and the response is collected at the normal direction without evanescent coupling to tapered fibers.

Interestingly, there exists a meaningful difference in the response of the high and medium molecular weight MEH-PPV polymers implemented in *conf-1H* and *conf-2M* microcavities. Thus, their temperature sensitivity is higher and temperature resolution lower in the high molecular weight polymer based devices. This dependence will be discussed in the next section.

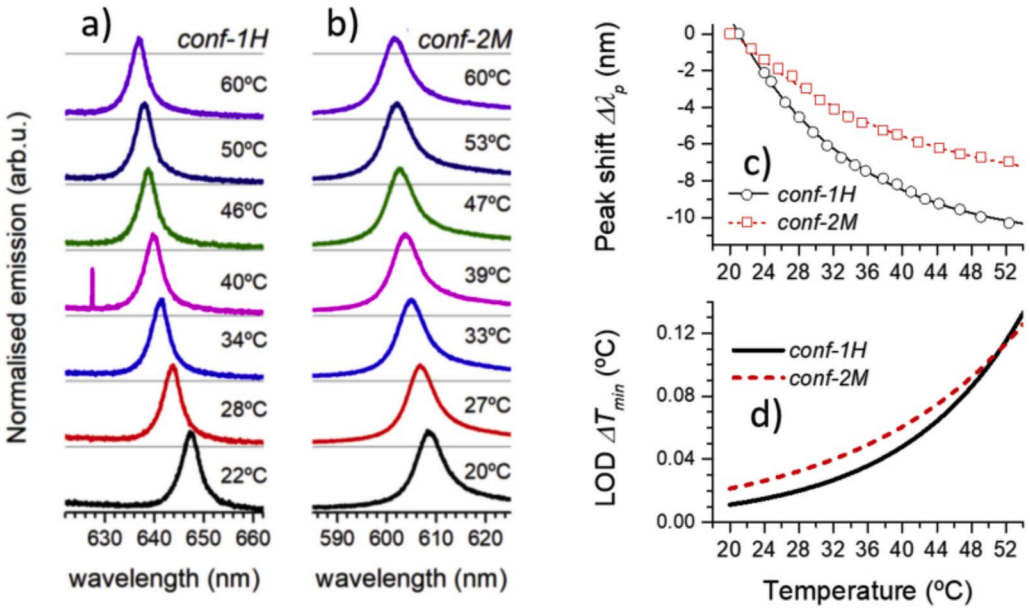

Fig. 4. Temperature evolution of normalized emission spectra of high (a) and medium (b) molecular weight MEH-PPV films within *conf-1H* and *conf-2M* microresonators, respectively. (c) Resonant peak shift $\Delta\lambda_p$ vs temperature (dots: experimental points; lines: least squares fits to experimental points) and (d) corresponding limit of detection of the microresonators acting as temperature sensors.

3.2. Optical modeling and thermo-optic coefficient determination

To simulate the large thermal wavelength shift of the emission band observed in the microresonators, we have used two different and independent approaches, namely, the classical transfer-matrix method to analyze the propagation of plane waves through a multilayer system using WVASE32 software package (J.A. Woollan Co.) and the finite element method for the evaluation of optical eigenmodes of the structure using COMSOL Multiphysics® software package. In both cases, the basic assumption in the performed analyses is that the wavelength position of the emission peak of the luminescent polymer incorporated to the FP cavity shifts mostly by the changes of the temperature dependent refractive index of the polymer layer incorporated to the resonator. To justify this assumption note that thermal expansion coefficient of the inorganic materials incorporated into the resonator are in the range of 10^{-6}-10^{-7} K^{-1} and their thermo-optic coefficient is positive and in the order of $\sim 10^{-5}$ K^{-1} [27]. On the other hand, the thermal expansion coefficient of polymers is in the range of 10^{-4}-10^{-5} K^{-1}, while their thermo-optic coefficient is in general negative with values in the range of -10^{-4} K^{-1} [28]. In particular, the linear thermal expansion coefficient reported for MEH-PPV is 3.2×10^{-4} K^{-1} [29] thus we expect a thickness expansion of about 1% for an increase of 30 K. Thus, it is a reasonable assumption to justify the observed resonant peak shifts reported in Fig. 4 to variations of the polymer refractive index with temperature.

3.2.1. Microresonator optical transmittance by classical transfer-matrix method

We have fitted the transmission spectra acquired at room temperature of the multilayer structure of the FP resonator within the transfer-matrix method traditionally used to study the propagation of electromagnetic waves through a stratified medium using WVASE32 software package. Within the fitting procedure, we have fixed the thickness of the polymer layer to the values observed by cross sectional SEM images, and the refractive index of MEH-PPV at 20 °C to 1.80, according to the reported values of the literature. This fitting procedure allows getting precise thickness and refractive index evaluation of all the layers within the resonators.

Then we have varied the refractive index of the polymer layer to reproduce the observed wavelength shifts of the resonant peak with temperature. Fig. 5a shows the result of this analysis. The simulations indicate that there is a linear correlation between the required refractive

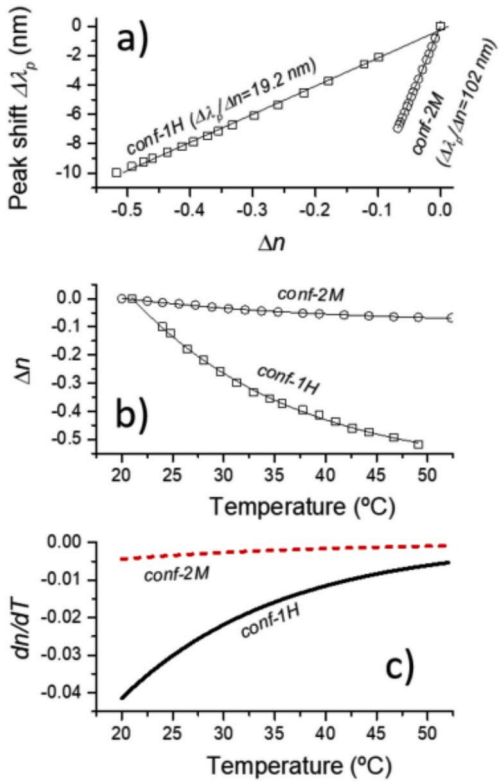

Fig. 5. (a) Refractive index variation Δn in the polymer layer within the resonator configurations considered in this work required to fit the observed resonant peak shift $\Delta\lambda_p$. (b) Correlation between Δn and temperature for *conf-1H* (squares) and *conf-2M* (circles) resonator configurations. (c) Thermo-optic coefficient *dn/dT* of the polymer layer incorporated in *conf-1H* and *conf-2M* resonators, according to the data above. The lines in (a) and (b) are least squares fits to the experimental data points.

index variation of the polymer layer and the position of the resonant peak, that takes the $\Delta\lambda_p/\Delta n$ values of 19.2 nm/RIU and 102 nm/RIU for *conf-1H* and *conf-2M* configurations, respectively. On the other hand, Fig. 5b shows the correlation between the obtained refractive index changes with respect to the temperature. Note that the slope of the regression of the experimental points included in this figure represent the thermo-optic coefficient of the polymer layer under analysis. Thus, it is found that *dn/dT* takes values reported in Fig. 5c, that, as average correspond to $-0.018\ K^{-1}$ and $-0.0022\ K^{-1}$ for the polymer layers incorporated in the *conf-1H* and *conf-2M* resonators, respectively.

3.2.2. Microresonator optical eigenmodes by finite element methods

Determination of the optical eigenmodes of the multilayer microresonators was performed by frequency domain analysis using finite element methods (FEM) with COMSOL Multiphysics® software package. Simulations of a nearly unidimensional model of the system considering the multilayer structure depicted in Fig. 1a, including the *BM1* and *BM2* Bragg mirrors and the defect layer comprising the MEH-PPV polymer film, were used to obtain the allowed optical states of the system for a range of polymer refractive index values. The assumption in this analysis is that the computed eigenmodes and the wavelength shifts of the stored energy profiles in a lossless cavity (i.e., without considering any loss in the elements of the multilayer structure) will correspond to those of the emission band of the resonator. Thus, there will be a correlation between the wavelength shifts of the allowed optical states in the microcavities and the refractive index change of the polymer within the multilayer structure.

In close agreement with the classical transfer-matrix analysis described above, the FEM simulations showed the same linear correlation between the refractive index change of the polymer layer and the position of the optical eigenmodes of the resonators, thus, confirming the dependence of the refractive index changes with respect to the temperature.

4. Discussion

As already mentioned, the position of the transmission band or allowed optical state within the resonator depends on the design of the multilayer structure, i.e., the thicknesses and the refractive indices of all the layers comprising the resonator, included the active polymer layer incorporated in the defect of the microcavity. A change in temperature of the system may produce a variation of both of the layer thicknesses and refractive indices of the resonator layers. Thus, an increase in temperature produces a positive thermal expansion and an increase of the refractive index of all the inorganic SiO_2 and Nb_2O_5 layers within the resonator. Both effects may produce a red shift on the emission of the resonator, as temperature increase, that is not observed experimentally. On the other hand, although an increase in temperature also produces a positive thermal expansion on the polymer film, the blue shift of the emitted radiation is only consistent with a strong decrease of the refractive index of the active polymer, as temperature increases, i.e., with negative thermo-optic coefficients for the polymer layers, as it is often the case when dealing with polymer thin films [28,30]. Besides, their absolute values are significantly higher than those reported for other polymers, and at the same time, it is found that they are strongly dependent on the molecular weight of the active polymer.

At this point, it is worth noting that within our experimental approach, the obtained values for the thermo-optic coefficient of the active MEH-PPV layers incorporated to the microresonators are independent of the refractive index considered for the active polymer layer at room temperature, or the initial position of the resonant peak of the FP resonator within the emission band of the active polymer. The evaluation of this parameter is based only on the relative wavelength shift of the emitted peak, within the assumptions described above for the two different optical modelling considered in section 3.2.

To justify the obtained strong dependence of the thermo-optic coefficient of MEH-PPV with temperature, other effects related to the light confinement in the FP resonator might not be discarded. Note that we have incorporated the active polymer layer within a cavity of a photonic crystal with significant Q-factor for the cavities. Thus, the Q-factor of *conf-1H* resonators have values around 150, while that of *conf-2M* resonators takes values around 90. Note, that higher quality factor for a resonant cavity are linked to stronger electric field localization within the photonic structure. Although it is not clear at the present moment for the authors if the presence of localization of electric fields within the FP resonator may affect the determination of the thermo-optical response of the polymeric film, it might not be discarded that the classical interpretation of thermo-optical response of the polymer considered in this work may be affected by them, especially if this localization effects are enhanced at the defect layer of the resonator, as it is the case in this study. To investigate if the space distribution of the electric field in the cavity of the microresonator has an influence on the thermal response of the devices, other microresonators with different locations of the MEH-PPV polymer layer within the defect *D* layer were built and their thermo-optical response was analyzed in similar conditions than in the other cases described below. A scheme of the series of manufactured resonators and the evaluated spatial electric field distributions within the multilayer devices are reported Fig. S2 of the supporting information file. It was found that, independently of its location within the *D* cavity (i.e., either at a maximum or a minimum of the electric field intensity evaluated at the wavelength of emission of the FP resonator), the blue shift of the resonant emission of the manufactured devices with the same molecular weight MEH-PPV polymer was nearly identical, thus supporting that the thermo-optical response of the polymeric films is not affected by the standing waves stablished within the FP resonator.

To sum up, the experimental results show a strong blue shift of the resonance emission mode of MEH-PPV microresonators when temperature increases. This blue shift has been interpreted because of the large thermo-optic coefficient of MEH-PPV layers. Therefore, the reported results indicate that this material could be interesting for thermal sensor applications. Moreover, as it has been already mentioned, MEH-PPV microresonators show high performance as compared to other optical sensors, in particular in terms of thermal sensitivity [17–21] and LOD [21–25]. Additionally, MEH-PPV microresonators show the advantage of monolithic integration capability on planar substrates, which is desirable for miniaturization processes. Besides, a high spatial resolution can be achieved if position microstages are implemented in the optical setup. Nevertheless, a limitation of MEH-PPV microresonators as temperature sensors is the temperature range and external conditions. The luminescence quenches at high temperature and under intense irradiation, which is common for most organic polymers, as opposed to inorganic optical sensors [31].

5. Conclusions

In this paper, it is reported that MEH-PPV films incorporated to the cavities of FP microresonators show negative thermo-optic coefficient of about $-0.018\ K^{-1}$ and $-0.0022\ K^{-1}$ for high and medium molecular weight polymers for the 20–60 °C temperature range. These values are consistent with theoretical simulations of optical transmittance by classical transfer-matrix method and the evaluation of the optical eigenmodes by finite element methods of the manufactured FP resonator cavities. These values are about the highest reported so far, to the best of our knowledge, and point to high performance optical thermal sensor applications. In particular, when acting as optical temperature sensors, the manufactured monolithic FP resonators show sensitivity of −0.22 nm/°C and −0.31 nm/°C for the medium and high molecular weight samples, respectively.

Declaration of competing interest

The authors declare that they have no known competing financial interests or personal relationships that could have appeared to influence the work reported in this paper.

CRediT authorship contribution statement

J. Gil Rostra: Writing - original draft, Data curation, Methodology, Investigation. **K. Soler-Carracedo:** Data curation, Conceptualization. **L. L. Martín:** Formal analysis, Conceptualization, Software. **F. Lahoz:** Project administration, Writing - review & editing. **F. Yubero:** Project administration, Writing - review & editing, Funding acquisition.

Acknowledgments

The authors thank financial support from Spanish MINECO-AEI (MAT2016-79866-R, MAT2016-75586-C4-4-P, IJCI-2016-30498), CSIC (201860E050) and EU-FEDER.

Appendix A. Supplementary data

Supplementary data to this article can be found online at https://doi.org/10.1016/j.dyepig.2020.108625.

References

[1] Burroughes JH, Bradley DDC, Brown AR, Marks RN, Mackay K, Friend RH, et al. Light-emitting diodes based on conjugated polymers. Nature 1990;347:539–41. https://doi.org/10.1038/347539a0.
[2] AlSalhi MS, Alam J, Dass LA, Raja M. Recent advances in conjugated polymers for light emitting devices. Int J Mol Sci 2011;12:2036–54. https://doi.org/10.3390/ijms12032036.
[3] Liu B, Lü X, Wang C, Tong C, He Y, Lü C. White light emission transparent polymer nanocomposites with novel poly(p-phenylene vinylene) derivatives and surface functionalized CdSe/ZnS NCs. Dyes Pigments 2013;99:192–200. https://doi.org/10.1016/j.dyepig.2013.04.038.
[4] Ye Q, Chi C. Conjugated polymers for organic solar cells. Sol. Cells - new Asp. solut. InTech; 2011. https://doi.org/10.5772/23275.
[5] Samuel IDW, Turnbull GA. Organic semiconductor lasers. Chem Rev 2007;107:1272–95. https://doi.org/10.1021/cr050152i.
[6] Alias AN, Zabidi ZM, Ali AMM, Harun MK, Yahya MZA. Optical characterization and properties of polymeric materials for optoelectronic and photonic applications. Int J Appl Sci Technol 2013;3.
[7] Bronstein H, Nielsen CB, Schroeder BC, McCulloch I. The role of chemical design in the performance of organic semiconductors. Nat Rev Chem 2020;4:66–77. https://doi.org/10.1038/s41570-019-0152-9.
[8] Morin P-O, Bura T, Leclerc M. Realizing the full potential of conjugated polymers: innovation in polymer synthesis. Mater Horiz 2016;3:11–20. https://doi.org/10.1039/C5MH00164A.
[9] Kiebooms R, Menon R, Lee K. Synthesis, electrical, and optical properties of conjugated polymers. In: Handb. Adv. Electron. Photonic mater. Devices. Elsevier; 2001. p. 1–102. https://doi.org/10.1016/B978-012513745-4/50064-0.
[10] Campoy-Quiles M, Etchegoin PG, Bradley DDC. On the optical anisotropy of conjugated polymer thin films. Phys Rev B 2005;72:045209. https://doi.org/10.1103/PhysRevB.72.045209.
[11] Koynov K, Bahtiar A, Ahn T, Cordeiro RM, Hörhold H-H, Bubeck C. Molecular weight dependence of chain orientation and optical constants of thin films of the conjugated polymer MEH-PPV. Macromolecules 2006;39:8692–8. https://doi.org/10.1021/ma0611164.
[12] Koynov K, Bahtiar A, Ahn T, Bubeck C, Hörhold H-H. Molecular weight dependence of birefringence of thin films of the conjugated polymer poly[2-methoxy-5-(2′-ethyl-hexyloxy)-1, 4-phenylenevinylene]. Appl Phys Lett 2004;84:3792–4. https://doi.org/10.1063/1.1739513.
[13] Johnson DI, Town GE. Refractive index and thermo-optic coefficient of composite polymers at 1.55 μm. In: Abbott D, Kivshar YS, Rubinsztein-Dunlop HH, Fan S, editors; 2005. p. 603821. https://doi.org/10.1117/12.656497.
[14] Town GE, Vasdekis A, Turnbull GA, Samuel IDW. Temperature tuning of a semiconducting-polymer DFB laser. In: 2005 IEEE LEOS Annu. Meet. Conf. Proc. IEEE; 2005. p. 778–9. https://doi.org/10.1109/LEOS.2005.1548231.
[15] McGehee MD, Heeger AJ. Semiconducting (conjugated) polymers as materials for solid-state lasers. Adv Mater 2000;12:1655–68. https://doi.org/10.1002/1521-4095(200011)12:22<1655::AID-ADMA1655>3.0.CO;2-2.
[16] Schwartz BJ. Conjugated polymers as molecular materials: how chain conformation and film morphology influence energy transfer and interchain interactions. Annu Rev Phys Chem 2003;54:141–72. https://doi.org/10.1146/annurev.physchem.54.011002.103811.
[17] Kajiya D, Koganezawa T, Saitow K. Hole mobility enhancement of MEH-PPV film by heat treatment at T g. AIP Adv 2015;5:127130. https://doi.org/10.1063/1.4939135.
[18] Lahoz F, Martín IR, Soler-Carracedo K, Cáceres JM, Gil-Rostra J, Yubero F. Holmium doped fiber thermal sensing based on an optofluidic Fabry-Perot microresonator. J Lumin 2019;206:492–7. https://doi.org/10.1016/j.jlumin.2018.10.103.
[19] Soler-Carracedo K, Ruiz A, Martín IR, Lahoz F. Luminescence whispering gallery modes in Ho3+ doped microresonator glasses for temperature sensing. J Alloys Compd 2019;777:198–203. https://doi.org/10.1016/j.jallcom.2018.10.297.
[20] Lahoz F, Martín IR, Gil-Rostra J, Oliva-Ramirez M, Yubero F, Gonzalez-Elipe AR. Portable IR dye laser optofluidic microresonator as a temperature and chemical sensor. Optic Express 2016;24:14383. https://doi.org/10.1364/OE.24.014383.
[21] Nawrocka MS, Liu T, Wang X, Panepucci RR. Tunable silicon microring resonator with wide free spectral range. Appl Phys Lett 2006;89:071110. https://doi.org/10.1063/1.2337162.
[22] Dong C-H, He L, Xiao Y-F, Gaddam VR, Ozdemir SK, Han Z-F, et al. Fabrication of high-Q polydimethylsiloxane optical microspheres for thermal sensing. Appl Phys Lett 2009;94:231119. https://doi.org/10.1063/1.3152791.
[23] Manzani D, Petruci JF da S, Nigoghossian K, Cardoso AA, Ribeiro SJL. A portable luminescent thermometer based on green up-conversion emission of Er3+/Yb3+ co-doped tellurite glass. Sci Rep 2017;7:41596. https://doi.org/10.1038/srep41596.
[24] Schartner E, Monro T. Fibre tip sensors for localised temperature sensing based on rare earth-doped glass coatings. Sensors 2014;14:21693–701. https://doi.org/10.3390/s141121693.
[25] Wade SA, Collins SF, Baxter GW. Fluorescence intensity ratio technique for optical fiber point temperature sensing. J Appl Phys 2003;94:4743. https://doi.org/10.1063/1.1606526.
[26] Ramakrishnan M, Rajan G, Semenova Y, Farrell G. Overview of fiber optic sensor technologies for strain/temperature sensing applications in composite materials. Sensors 2016;16:99. https://doi.org/10.3390/s16010099.
[27] Rose BA, Maker AJ, Armani AM. Characterization of thermo-optic coefficient and material loss of high refractive index silica sol-gel films in the visible and near-IR. Opt Mater Express 2012;2:671. https://doi.org/10.1364/OME.2.000671.
[28] Zhang Z, Zhao P, Lin P, Sun F. Thermo-optic coefficients of polymers for optical waveguide applications. Polymer (Guildf) 2006;47:4893–6. https://doi.org/10.1016/j.polymer.2006.05.035.
[29] Yan L, Yang F. Prediction and phase segregation in thin-film of conjugated polymer blends. J Polym Sci, Part B: Polym Phys 2005;43:1382–91. https://doi.org/10.1002/polb.20430.
[30] Foreman MR, Swaim JD, Vollmer F. Whispering gallery mode sensors. Adv Optic Photon 2015;7:168. https://doi.org/10.1364/AOP.7.000168.
[31] Runowski M, Shyichuk A, Tymiński A, Grzyb T, Lavín V, Lis S. Multifunctional optical sensors for nanomanometry and nanothermometry: high-pressure and high-temperature upconversion luminescence of lanthanide-doped phosphates—LaPO 4/YPO 4 :Yb 3+ –Tm 3+. ACS Appl Mater Interfaces 2018;10:17269–79. https://doi.org/10.1021/acsami.8b02853.